

EFFECT OF ROTOR BLADE ANGLE AND CLEARANCE ON BLOOD FLOW THROUGH A NON-PULSATILE, AXIAL, HEART PUMP

Matthew D. SINNOTT^{1*} and **Paul W. CLEARY**¹

¹ CSIRO Mathematical and Information Sciences, Clayton, Victoria 3169, AUSTRALIA

*Corresponding author, E-mail address: Matthew.Sinnott@csiro.au

ABSTRACT

This study involves CFD simulation of blood flow through a non-pulsatile, axial pump consisting of a complex multi-sectioned impeller with rotating and stationary components, and a stationary housing. We use a particle-based method, Smoothed Particle Hydrodynamics (SPH), to investigate the effects of varying the impeller blade pitch angle and the gap size between the rotor and housing. Regions of flow reversal are identified at the front and tail end of the pump. We show that the impeller blade inclination affects pump performance and the level of shear-related blood damage. The optimal blade angle was found to be for a pitch angle of 0°. The pressure rise across the pump, the flow rate and the shear losses are all shown to be affected by the inclusion of a rotor-housing clearance. This leads to flow losses that reduce the efficiency of the pump but also reduce the viscous energy losses in the pump.

INTRODUCTION

Ventricular assist devices (VADs) are used as a temporary bridge-to-transplant for patients with congestive heart failure, or as flow assistance for instances of heart disease where ventricular function is weakened. In 2004, it was estimated that more than 20 million patients worldwide suffer from heart failure (Behbahani et al., 2009). The number of patients requiring donor hearts is much larger than the available number of donors with waiting lists in excess of 2 years. Current VADs can provide life-support for only up to 2 years, prompting further developments in heart pump design to improve biocompatibility for long-term implantation. Reviews outlining developments in heart pump design and the role of CFD analysis can be found in Behbahani et al. (2009) and Wood et al. (2005).

Third generation VADs are being proposed as the leading technology for mechanical blood pumps (Wood et al., 2005) and consist of non-pulsatile centrifugal and axial flow pumps with impellers suspended by magnetic bearings so that component wear is reduced. Centrifugal type pumps generate high pressures at modest flow rates and use smaller impeller rotation speeds giving a gentler flow. In contrast, axial flow pumps produce a high flow rate at lower pressure. To maintain the desired flow rate, the impeller in an axial flow pump must operate at much higher speeds. Red Blood Cells (RBCs) may be potentially exposed to much greater degrees of shear stress in these devices but the residence time for RBCs (and thus exposure time) in this type of pump is much lower. Furthermore, axial pumps consume less power and are smaller making implantation easier.

Blood damage in artificial pumps occurs due to non-physiological flow conditions such as recirculation; high

or very low shear; flow separation; sharp-edged or rough pump geometry; narrow clearances; and stagnation regions. Blood damage refers to:

- *Haemolysis* which is leakage of haemoglobin from the cell rather than full membrane rupture. The RBC membrane is strained under shear to the point where pores open up in the membrane and leakage can occur into the surrounding plasma. This leakage reduces RBC life. Haemolysis depends on stress loading of the cell and exposure time.
- *Thrombosis* describes clot formation in regions of low shear such as recirculating flow. Clots can grow in size inside the pump modifying the flow field, or can break off and travel into the circulatory system.

RBCs have good resistance to the shear stress levels found in the circulatory system, which can be as large as 50 Pa in diseased arteries. The high impeller speeds in axial pumps can expose RBCs to peak shear stresses of up to 1 kPa. Currently there are no models that reliably link flow behaviour such as stress and shear rate to clinical markers for blood damage (Goubergrits, 2006). Instead some authors (Arora et al., 2003; Chua et al., 2007; Jones 1995) have set threshold levels for likely damage based on peak stress levels. Others have proposed a strain model (Behbahani et al. 2009) that takes into account the RBC deformation history, but this requires the RBC geometry to be taken into account for the CFD models.

CFD has been used in the heart pump industry for more than a decade, and is a well-established tool for pump optimisation. To date, this has only involved grid-based methods and almost entirely focused on studying steady flow conditions; for example, Untaroiu et al. (2005) and Chua et al. (2007). Models of transient flow are necessary for designers to understand the velocity and pressure fluctuations occurring in a pump under unsteady flow conditions as would occur in a clinical, *in vivo* setting.

An alternative to modelling biomedical flows on a structured grid is Smoothed Particle Hydrodynamics (SPH). It is a transient, Lagrangian CFD method that does not use a grid. Instead computations are performed on the SPH ‘particles’ which travel with the flow carrying local state information with them. A benefit is that there is no need for a slip mesh to manage moving components in the flow as sometimes used in grid-based methods, nor the potential mass and energy losses associated with flow from moving mesh to stationary mesh. In SPH, boundary geometries of almost arbitrary complexity may be included such as the VAD rotor geometry. SPH particles can carry fluid history easily enabling us to include a strain based model for blood cell damage. SPH also enables rule-based modification of particles, meaning that one could also potentially model the growth of thrombi

inside the pump. This is very hard for traditional grid-based methods and would enable investigation of critical medical problems well beyond the scope of traditional solvers. So part of the motivation for using SPH here, lies in the future deployment of the advantages described above. Despite the potential benefits of the SPH method for studying biomedical systems, very few SPH models of biological flows have so far been attempted, with the exception of an arterial flow study by Sinnott et al. (2006). The aim here is to use SPH to develop an understanding of the flow of blood through an axial flow heart pump. The effect of important aspects of pump geometry on the flow field, pressure distribution, viscous energy losses and pump performance are examined.

MODEL DESCRIPTION

Smoothed Particle Hydrodynamics

The SPH method (Monaghan 2005) involves converting the Navier-Stokes partial differential equations into ordinary differential equations via a spatial discretisation. The interpolated value of a function A at any position \mathbf{r} can be expressed using SPH smoothing as:

$$A(\mathbf{r}) = \sum_b m_b \frac{A_b}{\rho_b} W(\mathbf{r} - \mathbf{r}_b, h) \quad (1)$$

Where m_b and \mathbf{r}_b are the mass and density of particle b and the sum is over all particles b within a radius $2h$ of \mathbf{r} . Here $W(\mathbf{r}, h)$ is a C^2 spline based interpolation or smoothing kernel with radius $2h$ that approximates the shape of a Gaussian function. The gradient of the function A is given by differentiating the interpolation equation (1) to give:

$$\nabla A(\mathbf{r}) = \sum_b m_b \frac{A_b}{\rho_b} \nabla W(\mathbf{r} - \mathbf{r}_b, h) \quad (2)$$

From Monaghan (1992), the SPH continuity equation is:

$$\frac{d\rho_a}{dt} = \sum_b m_b (\mathbf{v}_a - \mathbf{v}_b) \bullet \nabla W_{ab} \quad (3)$$

where ρ_a is the density of particle a with velocity \mathbf{v}_a and m_b is the mass of particle b . We denote the position vector from particle b to particle a by $\mathbf{r}_{ab} = \mathbf{r}_a - \mathbf{r}_b$ and let $W_{ab} = W(\mathbf{r}_{ab}, h)$ be the interpolation kernel with smoothing length h evaluated for the distance $|\mathbf{r}_{ab}|$. This form of the continuity equation is Galilean invariant (since the positions and velocities appear only as differences), has good numerical conservation properties and is not affected by free surfaces or density discontinuities.

The momentum equation can be written as:

$$\frac{d\mathbf{v}_a}{dt} = \mathbf{g} - \sum_b m_b \left[\begin{pmatrix} \left(\frac{P_b}{\rho_b^2} + \frac{P_a}{\rho_a^2} \right) \\ -\frac{\xi}{\rho_a \rho_b} \frac{4\mu_a \mu_b}{(\mu_a + \mu_b)} \frac{\mathbf{v}_{ab} \mathbf{r}_{ab}}{\mathbf{r}_{ab}^2 + \eta^2} \end{pmatrix} \nabla_a W_{ab} \right] \quad (4)$$

where P_a and μ_a are pressure and fluid viscosity of particle a and $\mathbf{v}_{ab} = \mathbf{v}_a - \mathbf{v}_b$. ξ is a factor associated with the viscous term (Cleary et al. 2007), η is a small parameter and \mathbf{g} is the gravity vector.

We use a quasi-compressible formulation (near the incompressible limit) with an equation of state to give the relationship between particle density and fluid pressure. A suitable one is:

$$P = P_0 \left[\left(\frac{\rho}{\rho_0} \right)^\gamma - 1 \right] \quad (5)$$

where P_0 is the magnitude of the pressure and ρ_0 is the reference density. For water or blood we use $\gamma = 7$. This pressure is then used in the SPH momentum equation (4) to give the particle motion.

The Reynolds number for flow through adult axial flow VADs is typically in the turbulent regime ($\sim 10^4$) due to high impeller speeds (Untaroiu et al. 2005). SPH formally resolves all length scales of the flow above the resolution length; much like a Large Eddy simulation. However, there is no formal turbulence modelling since the present SPH formulation does not have a sub-grid scale model.

Pump Performance

Pumps are typically designed to operate at a specific pressure for a given flow rate and at a specific impeller speed. Physiological pressures are between 80-140 mmHg (10.6-18.6 kPa). Ventricular devices aim to support the heart which delivers a flow rate of 5 L/min. Typical flow rates for axial flow pumps are in the range 2-10 L/min (Untaroiu et al. 2005). Following Brennen (1994) we define pump efficiency as:

$$\eta_H = \frac{dV}{dt} \frac{\Delta P}{M_z w} \quad (6)$$

where dV/dt is the volumetric flow rate, M_z is the impeller torque, ΔP is the pressure rise across the pump and w is the impeller rotation rate in rad/s.

Axial Flow Heart Pump Geometry

The LEV-VAD pump rotor and housing (similar to Untaroiu et al. 2005) are shown in Figure 1. The rotor consists of three components: 1) a stationary inducer with 6 blades to maintain the linear flow of blood; 2) a rotating impeller with 3 blades of varying pitch that applies a high angular acceleration to the blood; and 3) a stationary diffuser with 3 blades to convert the rotational flow back into a linear flow before it exits the pump. A typical rotor speed of 5000 rpm was chosen for the simulations.

To minimise the size of the computational domain for this model, we apply periodic boundary conditions at the inlet and outlet of the pump so that flow out of the outlet is channelled back in through the inlet. A 5 mm long region with a high specified drag was located inside the housing immediately in front of the inlet in order to provide a pressure resistance equivalent to its operating load for the pump to work against. In order to fill the pump with fluid, a side channel was added to the housing just before the inducer and an inflow was attached to the end of the channel. Fluid was fed into the system until the pump was pressurised at a target pressure of 10 kPa.

The viscosity used was 0.0037 Pa.s and the density was 1000 kg/m³, approximating the properties of blood. The SPH particle spacing was 0.5 mm, corresponding to around 300,000 fluid particles in a simulation. The flow rate through the pump and the torque on the impeller were monitored until they became steady. Data was then collected over 0.24 s (20 revolutions of the impeller).

Three impeller blade pitch angles were used:

- A base case with 0°
- 20° inclined backwards into the flow
- 20° inclined forwards.

For these cases the blade tip was set flush with the outer wall. A fourth case with the same blade inclination as the base case but with a 1 mm clearance between the tip of the impeller blade and the housing was also examined.

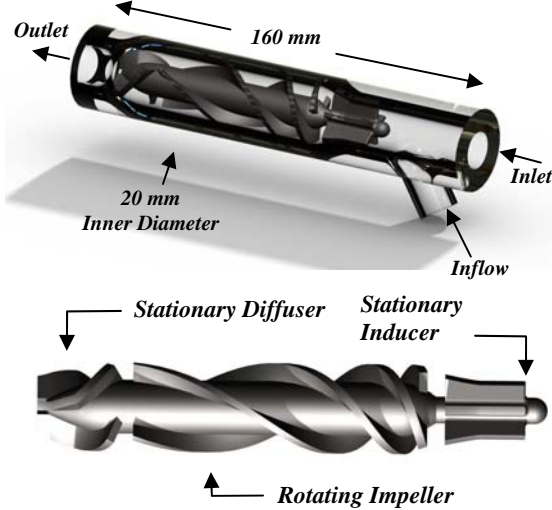


Figure 1: Diagram of heart pump showing LEV-VAD style rotor and housing. The rotor with variable pitch blades is shown separately at the bottom.

PREDICTIONS OF FLOW IN THE PUMP

Base Case

In this study 3D simulations of flow through the pump were performed and details of the flow were collected onto a regular Cartesian grid to give long-term averaged quantities for basic characterisation of the flow.

The long-term averaged flow predictions for the base simulation are presented in Figure 2. Tangential (v_t) and axial (v_z) velocity fields are shown in Figures 2a&b, respectively. Blood enters the inducer (at the start of the pump rotor) at speeds of 0.7-0.8 m/s. The flow decelerates in the axial direction upon entering the impeller whose rotation then accelerates the flow in the circumferential direction. The varying pitch of the impeller (and the incremental change in the angle of attack of the blade) leads to an increase in tangential speed with axial distance along the impeller. The tangential speed also increases with radial distance away from the centre of the impeller. For example, at the surface of the impeller shaft tangential speeds of 2.5 m/s are observed. This rises to about 5 m/s at the outer wall. The tangential flow speeds are consistent with the increase in blade edge speed with radial distance. The flow exits the rotating impeller into the stationary diffuser blades. These are curved in the opposite direction to the impeller blades. Their role is to dissipate the angular motion of the fluid so that it is directed linearly out of the pump. The deceleration of the high speed rotational flow generates a large pressure head at the end of the pump. This drives the flow forwards and out of the pump at an appropriate flow rate and pressure for cardiac assistance.

Theoretical pump design currently involves matching blade angles between the impeller and diffuser. This is to optimise the transfer of flow between the two pump regions. However, pressures and flow velocities change considerably between them. It is not enough to assume that the bulk flow simply follows the surface geometry of the rotor. Figure 2a shows that the flow is more complex

in the entrance and exit to the impeller. Viscous shear between fluid layers is responsible for blood, at a distance from the moving blades, rotating with the blade. High tangential velocities are observed between the inducer and impeller blades. Also the damping of the rotational component of the flow at the diffuser does not occur instantaneously for fluid exiting the impeller. High tangential velocities are observed well inside the diffuser region and concentrated near the housing. This highlights the need for detailed flow simulations to better understand the influence of complex pump geometry on the flow field.

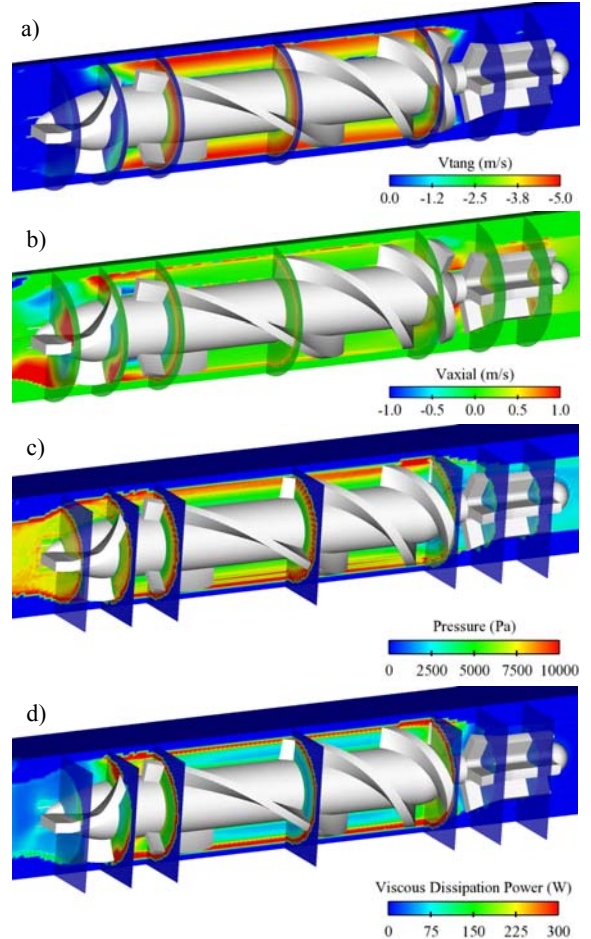


Figure 2: Average a) tangential and b) axial flow velocities, c) pressure, and d) viscous dissipation power within the pump housing for the base simulation.

Axial flow inside the impeller is highest in a narrow annular region adjacent to the housing wall. Axial speeds increase significantly for flow exiting the impeller into the diffuser since the rotational kinetic energy is used to accelerate the flow in the axial direction. This results in an increase in pressure inside the diffuser. Some fluid is forced backwards into the impeller along the surface of the rotor shaft. Flow between the stationary diffuser blade and the moving impeller blade therefore introduces an unsteady recirculation between the impeller and diffuser.

Figure 2c shows that the pressure distribution is non-uniform throughout the pump. Pressure is relatively low (2.5 kPa) in the inducer. There is a significant pressure rise inside the impeller. The highest pressures are in excess of 10 kPa and are concentrated in a small annular region adjacent to the outer wall. At the outlet, the

pressure is 7.5 kPa in the central region of the flow, and 10 kPa near the outer wall. The total pressure delivered by the pump is about 8.5 kPa which equates to a clinical pressure of 64 mmHg.

The viscous dissipation power is shown in Figure 2d and is a prediction of the energy losses in the fluid due to viscous shear. While there are no currently accepted models for relating predictions of shear (or strain) to clinical measurements of haemolysis it is believed that regions of strong shear are potential sites for RBC damage. It is useful from a pump design perspective to therefore identify pump geometry characteristics that are responsible for regions of high shear dissipation. The dominant shear energy losses in this pump are concentrated in a narrow layer adjacent to the housing. This is because axial and tangential speeds are zero at the wall. Two regions of moderate shear energy loss are predicted:

- 1) between the inducer and the impeller; and
- 2) between the impeller and diffuser, with high shear losses predicted along the outer radial half of the front edge of the diffuser blades.

These are locations of significant flow deceleration that lead to shearing of fluid layers near the pump components.

Recirculation in the Diffuser / Impeller region

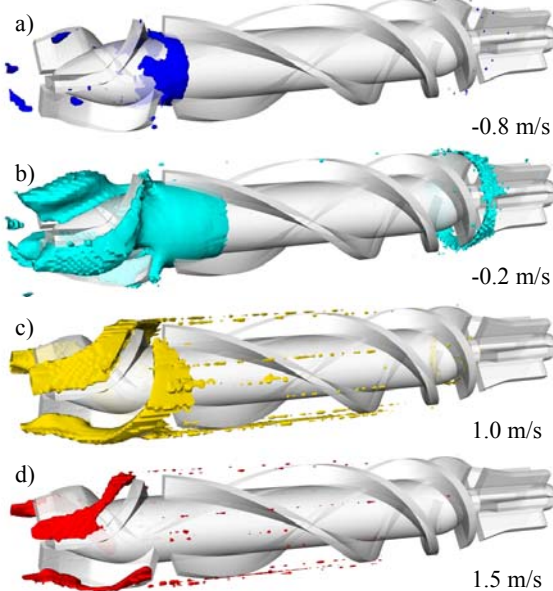


Figure 3: Isosurfaces of axial velocity (V_z) demonstrating retrograde flow in the pump for a) -0.8 m/s, b) -0.2 m/s, c) 1.0 m/s, and d) 1.5 m/s. These are for the base simulation.

Flow, exiting the rotating impeller into the stationary diffuser blades, can result in a recirculation of blood between the diffuser and impeller. This has been observed by other authors (Chua et al 2007) in similar axial flow pumps. As an impeller blade moves past a diffuser blade, flow exiting the impeller will be split by the stationary blade. Some of the flow will be reflected off of the rear of the diffuser blade and is directed back into the impeller. Regions of recirculation are of concern for pump designers as they can trap blood inside the pump increasing the exposure time for RBCs to significant levels of shear and increasing the potential for blood damage.

Four isosurfaces of axial velocity, V_z , are shown in Figure 3. Figure 3a show that there is significant retrograde flow occurring within this pump at speeds of up to at least 0.8 m/s. This reverse flow extends to the diffuser exit along the rear side of the diffuser blades. Figure 3b shows that reverse flow is also observed well into the impeller (about 1/5 of the impeller length) and lies predominantly along the surface of the impeller shaft. Figure 3b also shows some flow reversal in the inducer-impeller region but this flow is at slower speeds than observed in the impeller-diffuser. Figures 3c&d show that the antegrade flow in the diffuser region is directed along the front of the blades. Moderate axial speeds (1.0 m/s) are observed near the surface of the diffuser blades, and at a larger radial distance near the housing. There is also a compact 1.5 m/s jet of higher speed fluid a small distance above the curved blade surface. This indicates that there is some shearing of the flow in the entrance of the diffuser.

Effect of Impeller Blade Pitch Angle

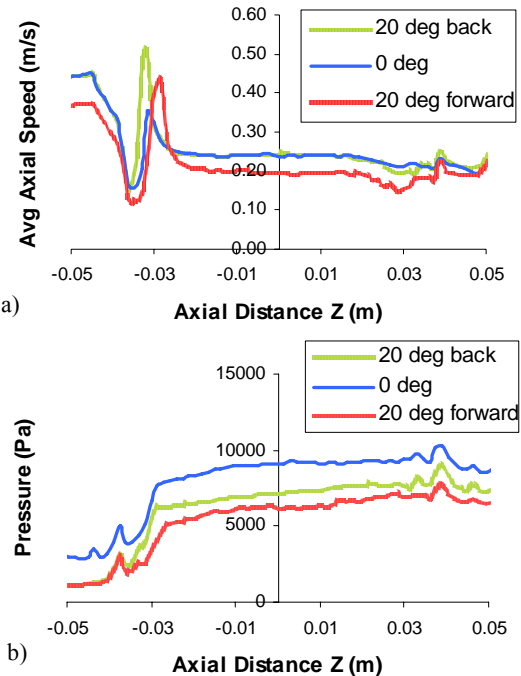


Figure 4: Average a) axial speed and b) pressure along the length of the pump, for the three blade angles.

Varying the blade pitch angle causes modification of the flow through the pump. The tangential and radial speeds do not alter significantly, but there are important changes to the axial speed and pressure distribution (see Figure 4). The axial speeds in the impeller and diffuser regions are about 20% lower for the case where the blade is inclined forwards with the flow. The inducer/impeller transit region shows a sudden acceleration in the axial direction for flow exiting the inducer. This is immediately before the strong axial deceleration when fluid begins to interact with the impeller blades. The location of the peak axial speed and its magnitude also change with the impeller blade angle. The pitch angle controls how much of the blade geometry lies inside the region between the inducer and impeller. Both the backward and forward inclined blade angles have higher axial speeds in the region between the inducer and impeller than does the normal directed blade angle. The rapid flow acceleration and deceleration results in shearing of fluid layers at the

impeller entrance. Moderate levels of viscous dissipation are therefore observed at the entrance to the impeller.

The pressures inside the pump (Figure 4b) vary considerably with the blade angle. Both the inclined angles have lower pressures throughout the pump than does the base case. The 20° backwards inclined case has 20% lower pressures in the impeller region while the forward inclined case has about 30% lower pressure. The pressure rise across the pump for each case is summarised in Table 1 and will be discussed at the end of this section. The distribution of viscous energy dissipation is similar throughout the pump except in the inducer-impeller. Figure 5 shows a side-on clipped view of the viscous power distribution in the 1st half of the pump. For the 20° backwards case, high levels of shear energy loss are observed extending from the base of the impeller blade up to the top of the inducer blade following the angle of the blade. This suggests that the reverse inclination of impeller blades could lead to higher blood damage in this region. Shear losses are still significant in the base case and occur within a compact region around the blade, extending a short distance into the impeller region. For the 20° forwards case, energy losses in the gap between the inducer and impeller are much milder and the high loss region adjacent to the blade in the impeller region becomes more compact.

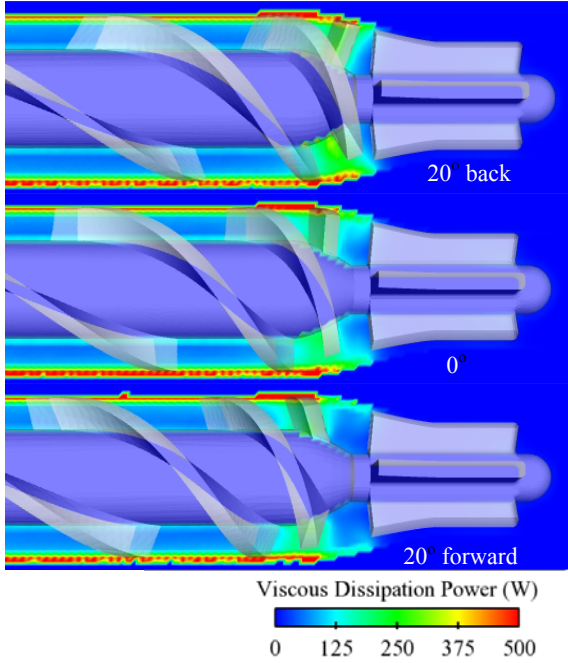


Figure 5: Viscous dissipation power in the inducer-impeller region for the different blade angle cases a) 20° inclined backwards; b) base case; and c) 20° forwards.

For each blade angle, Table 1 lists details of the predicted volumetric flow rate (dV/dt), impeller torque (M_z), impeller power (p_z), pressure rise across the pump (ΔP) and hydraulic efficiency (η_H).

The volumetric flow rate is highest for the 0° case at almost 2 L/min. The backwards inclined blade has a 10% lower flow rate, while the forwards inclined blade is 20% lower. Impeller torque and power are highest for the backwards inclined case as this impeller must do more work in pushing blood through the pump. The forwards

inclined blade has a 10% lower torque and does about 10% less work than the 0° case.

	dV/dt (L/min)	M_z ($\mu N.m$)	p_z (W)	ΔP (kPa)	η_H (%)
20° back	1.80	7.37	3.86	6.2	4.8
0°	1.98	7.13	3.73	5.9	5.2
20° forward	1.62	6.47	3.39	5.4	4.3

Table 1: Effect of impeller blade inclination on pump performance

The pressure rise across the pump is highest for the backwards inclined blade, but it has a smaller pumping efficiency than the 0° case based on its lower flow rate. The forwards inclined blade predicts a smaller pressure differential and even lower pumping efficiency.

To summarise, inclining the impeller blade backwards towards the inlet leads to higher pressures in the pump and the potential for greater blood damage at the impeller entrance. There is a mild drop in flow rate (and pumping efficiency) compared with the base case. Inclining the blade forwards appears to reduce blood damage risk but also reduces the flow rate (and pumping efficiency) further. The optimal case appears to be for a pitch angle of 0° . Reported shear losses in the impeller entrance are small. Its flow rate and pumping efficiency are the highest of the three geometries considered.

Effect of rotor clearance

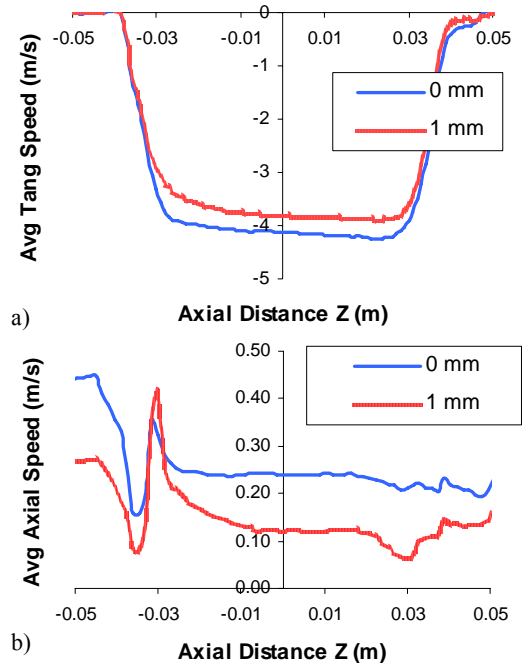


Figure 6: Average a) tangential and b) axial velocities along the pump for a 0 mm gap (blue) and 1 mm gap (red).

A 1 mm clearance between the impeller blades and the inner wall of the pump housing has a significant impact on the flow performance of the pump. Figure 6 shows how the tangential and axial flow varies along the pump for the base case (which has 0 mm clearance between impeller blade and housing) and for the case with the 1 mm gap. Tangential speed increases with distance along the impeller for both cases due to acceleration by the variable pitch blades. However, the gap results in a mild decrease

(7-10%) in tangential speed in the impeller region. The difference is only mild because fluid in the gap is still strongly accelerated by shear from adjacent fluid layers that are in contact with the edge of the blade. The average axial speed at the inlet, and inside the impeller and diffuser for the 1 mm gap is around half that of the “no gap” case. The gap introduces flow leakage into the impeller region which reduces the flow speed through the pump (and the pumping efficiency).

Figure 7a shows the pressure distribution for the two gap sizes. The 1 mm gap has lower pressures throughout the pump compared to the no gap case. The impeller region shows the best example of this with a 50% reduction in pressure. The sharp rise and fall of axial speed between the inducer and impeller (Figure 6b) corresponds to the increase of pressure in this region. Figure 7b shows the viscous dissipation along the pump. The reduction in axial and tangential speeds leads to smaller velocity gradients and lower amounts of shear. A decline in dissipation rate of 30% is found in the impeller region for the 1 mm gap.

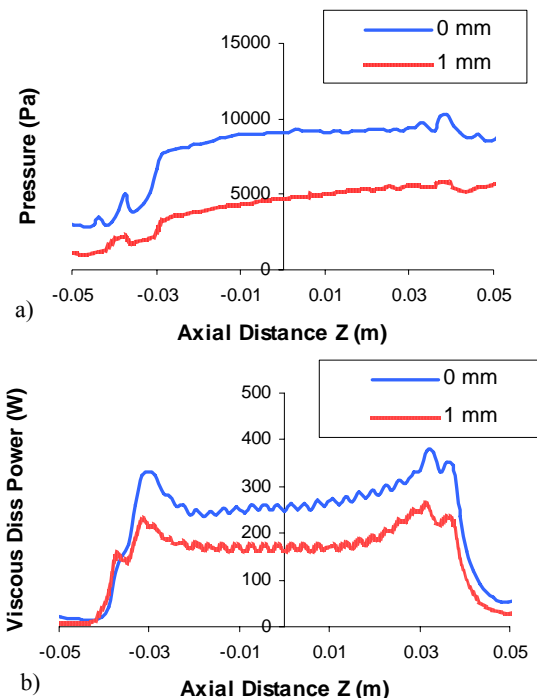


Figure 7: Average a) pressure and b) viscous dissipation along the pump for a 0 mm gap (blue) and 1 mm gap (red).

Table 2 summarises pump performance for the cases with and without impeller-housing gap and shows the significant effect of a 1 mm gap. The torque and corresponding power draw are much lower for the impeller with the gap due to flow leakage through the gap. The pressure rise across the pump is around 25% smaller and leads to a reduced volumetric flow rate (by 35%) and a 30% lower pumping efficiency. The gentler flow though is likely to reduce the risk of blood damage.

	dV/dt (L/min)	M_z ($\mu N.m$)	p_z (W)	ΔP (kPa)	η_H (%)
0 mm gap	1.98	7.13	3.73	5.9	5.2
1 mm gap	1.32	5.28	2.77	4.5	3.6

Table 2: Effect of impeller-housing clearance on pump performance.

CONCLUSION

A 3D SPH model of an axial flow pump has been developed. Some flow reversal was identified at the entrance and exit of the impeller. The effect of impeller blade geometry on the local flow field, pressures, energy losses and pump performance has been studied. A pitch angle of 0° was found to give the best pump performance. Inclining the impeller blade backwards generated a higher pressure differential across the pump but a lower flow rate leading to lower pumping efficiency and a mild increase in power used. Higher shear could potentially lead to higher incidence of shear-induced blood trauma. Inclining the blade forwards led to a lower pressure differential, a lower flow rate and a corresponding reduction in pump efficiency. A 1 mm gap between the impeller blades and the housing resulted in substantially lower pressures inside the pump and a 30% drop in pump efficiency, with less power required to drive the impeller and a predicted decrease in blood damage through viscous shear. Future studies will aim to better match real pump efficiencies (15-30%) and investigate the effect of rotation speed on pump performance.

REFERENCES

- ARORA, D., BEHR, M. and PASQUALI, M., (2003), “Blood damage measures for ventricular assist device modelling”, in *Moving Boundaries VII*, 129-138, Wit Press Publishing.
- BEHBAHANI, M., BEHR, M., HORMES, M., STEINSEIFER, U., ARORA, D., CORONADO, O. and PASQUALI, M., (2009), “A review of computational fluid dynamics analysis of blood pumps”, *Euro. J. of Applied Mathematics*, **20**, 363-397.
- BRENNEN, C.E., (1994), “Hydrodynamics of Pumps”, Concepts NRMC and Oxford Uni Press.
- CHUA, L.P., SU, B., TAU, M.L. and TONGMING, Z., (2007), “Numerical Simulation of an Axial Blood Pump”, *Artificial Organs*, **31**, 560-570.
- CLEARY, P.W., PRAKASH, M., HA, J., STOKES, N. and SCOTT, C., (2007), “Smooth particle hydrodynamics: status and future potential”, *Progress in Computational Fluid Dynamics*, **7**, 70-90.
- GOUBERGRITS, L., (2006), “Numerical modelling of blood damage: current status, challenges, and future prospects”, *Expert Rev. Med. Devices*, **3**, 527-531.
- JONES, S.A., (1995), “A Relationship between Reynolds Stresses and Viscous Dissipation: Implications to Red Cell Damage”, *Annals of Biomed Eng*, **23**, 21-28.
- MONAGHAN, J. J., (2005), “Smoothed Particle Hydrodynamics”, *Rep. Prog. Phys.*, **68**, 1703-1759.
- SINNOTT, M.D. and CLEARY, P.W. (2006). “An investigation of pulsatile blood flow in a bifurcation artery using a grid-free method”, *Proc. Fifth International Conference on CFD in the Process Industries*, Melbourne.
- UNTAROIU, A., THROCKMORTON, A.L., PATEL, S.M., WOOD, H.G., ALLAIRE, P.E. and OLSEN, D.B., (2005), “Numerical and Experimental Analysis of an Axial Flow Left Ventricular Assist Device: The Influence of the Diffuser on Overall Pump Performance”, *Artificial Organs*, **29**, 581-591.
- WOOD, H.G., THROCKMORTON, A.L., UNTAROIU, A. and SONG, X., (2005), “The medical physics of ventricular assist devices”, *Rep. Prog. Phys.* **68**, 545-576.